Time-lapse monitoring of rock properties with coda wave interferometry

Alexandre Grêt[†], Roel Snieder[†] and John Scales[‡]
[†] *Center for Wave Phenomena, Department of Geophysics, Colorado School of Mines, CO 80401, USA*
[‡] *Physical Acoustics Lab, Colorado School of Mines, CO 80401, USA*

ABSTRACT
The coda of a waveform consists of that part of the signal after the directly arriving phases. In a finite medium, or in one that is strongly heterogeneous, the late time coda is dominated by waves which have repeatedly sampled the medium. Small changes in a medium which might have no detectable influence on the first arrivals may be amplified by this repeated sampling and thus made visible in the coda. We refer to this use of multiple-sampling coda waveforms as *Coda Wave Interferometry*. We have exploited ultrasonic coda waves to monitor time-varying rock-properties in a laboratory environment. We have also studied the dependence of velocity on uni-axial stress in Berea sandstone, the non-linear temperature dependence of velocity in granite and the change in velocity due to an increase of water saturation in sandstone. There are many other possible applications of Coda Wave Interferometry in geophysics, including dam and volcano monitoring, time-lapse reservoir characterization, and rock physics.

Key words: velocity estimation, coda wave, multiple scattering, time-lapse, rock physics, acoustic emissions, fluid saturation

Introduction

Geophysicists investigate the structure of the subsurface by making indirect measurements on the surface and relating them to those predicted by theoretical Earth models. The Earth, however, is a highly complex system, and we almost always have to simplify our models in order to make them tractable. In many applications, this simplification means treating unmodeled physics as noise, with the result that information contained in the data is discarded. For seismic data, this typically means ignoring the coda waves that make up the tail of a seismogram. (In music the coda is the concluding passage of a movement or composition (Latin *cauda*, tail).) Geophysical applications based on use of the coda waves include earthquake prediction (Aki, 1985; Sato, 1988), volcano monitoring (Aki, 2000; Fehler *et al.*, 1998) or monitoring of temporal changes in the subsurface (Chouet, 1979; Revenaugh, 1995)(see also (Aki & Chouet, 1975).)

Consider the following examples: in monitoring a nuclear waste disposal site, one is not primarily interested in imaging the site. However, it is critical to monitor temporal changes in the site. In recent years, applied geophysicists have spent much effort on time-lapse seismology to monitor hydrocarbon reservoirs during recovery operations. Hydrocarbons move in the subsurface, reservoir rocks are artificially fractured, water-oil horizons move and steam propagates through the reservoir (Lumley, 1995; Wang, 1997). The high sensitivity of coda waves to small perturbations of the medium, makes them a powerful tool to monitor these kinds of changes.

We present four laboratory experiments in which we monitor the change in seismic velocity resulting from a change in uni-axial stress in a sample of Berea sandstone, from a temperature change in a sample of Elberton granite, a sample of aluminum and from a change in water saturation in a sample of Berea sandstone. We excite and record ultrasonic waves and extract the velocity change from the coda waves.

Sensitivity of Coda Waves

In a tomographic transmission experiment, the area under investigation is usually sampled once. The traversing waves have a certain sensitivity (depending on distance, velocity, sampling) to a velocity change in this area. In a coincident-source-receiver reflection experiment the same area is sampled twice and is therefore twice as sensitive to a velocity change than in the transmission case. In a setup where a wave is bouncing back and forth, and samples the same area multiple times, the experiment becomes more and more sensitive to a velocity change. This amplification of a velocity change, due to the multiple sampling of the same area is the key idea we use in this paper. In the laboratory this multiple sampling can be achieved in many ways. The above example can be thought of as a "bouncing ball mode". In a cylinder, we can have a surface wave that travels around the circumference many times. There are geometries where the wave-modes are less obvious to understand but the amplification concept remains the same.

In the case where a wave samples a certain area only once we can still have an amplification effect provided the area under investigation contains multiple small-scale changes, such as colloidal suspensions, clouds of bubbles or grains in a rock. In this case all the small-scale changes give rise to a long scattered wave path with a high sensitivity to velocity changes.

Multiply scattering or bouncing ball mode?

In a multiply scattering regime, we can write the wave-field in terms of a Feynman path summation (Snieder, 1999). For a change in the wave velocity, for quasi-random perturbations of the point scatterer location, or for a change in the source location, we can estimate this perturbation from multiply scattered waves by a cross-correlation in the time domain (Snieder *et al.*, 2002). We refer to the waveform before the perturbation as the unperturbed signal, and to the waveform after the perturbation as the perturbed signal. The unperturbed wave-field can be written as a Feynman path summation over all possible paths P (Snieder, 1999):

$$u_{\rm unp}(t) = \sum_P A_P S(t - t_P), \tag{1}$$

where a path is defined as a sequence of scatterers encountered by the wave, t_P is the travel time along path P, A_P is the corresponding amplitude and $S(t)$ is the source wavelet. The sum over paths contains a sum over all possible mode conversions (P-waves, S-waves and surface waves), and it describes both paths that bounce off the free surface and/or paths that connect scatterers.

When the background velocity is perturbed, the dominant effect on the waveform arises from the change in the travel time τ of the wave that travels along each path:

$$u_{\rm per}(t) = \sum_P A_P S(t - t_P - \tau_P). \tag{2}$$

We can compute the time-windowed correlation coefficient between the unperturbed and the perturbed signal from:

$$R^{(t,T)}(t_s) \equiv \frac{\int_{t-T}^{t+T} u_{\rm unp}(t')\, u_{\rm per}(t'+t_s)dt'}{(\int_{t-T}^{t+T} u^2_{\rm unp}(t')dt' \int_{t-T}^{t+T} u^2_{\rm per}(t')dt')^{\frac{1}{2}}}, \tag{3}$$

where the time window is centered at time t with duration $2T$ and t_s is the time shift used in the cross-correlation. When the perturbed and unperturbed wave fields defined by equations (1) and (2) are inserted into (3), double sums over all paths appear. The cross-terms with different paths ($P \neq P'$) are incoherent and average out to zero when the mean of the source signal vanishes. We can therefore approximate the time-windowed correlation coefficient by:

$$R^{(t,T)}(t_s) \approx \frac{\sum_{P(t,T)} A_P^2\, C(\tau_P - t_s)}{\sum_{P(t,T)} A_P^2\, C(0)}, \tag{4}$$

where the sum is taken over the paths with arrival times within the time window of the cross-correlation, and the auto-correlation of the source signal is defined as

$$C(t) \equiv \int_{-\infty}^{\infty} S(t'+t)S(t')dt'. \tag{5}$$

For time shifts τ much smaller than the dominant period, a second-order Taylor expansion gives $C(\tau) = C(0)(1 - \frac{1}{2}\overline{\omega}^2\tau^2)$, where $\overline{\omega}^2$ is the mean-squared frequency of the waves that arrive in the time window. Using this in equation (4) we can write

$$R^{(t,T)}(t_s) = 1 - \frac{1}{2}\overline{\omega}^2 \left\langle (\tau - t_s)^2 \right\rangle_{(t,T)}, \tag{6}$$

where $\langle \cdots \rangle_{(t,T)}$ stands for the average over the wave paths with arrivals in the time interval $(t-T, t+T)$.

The time shifted cross-correlation $R^{(t,T)}(t_s)$ has a maximum when

$$t_s = t_{\rm max} \equiv \langle \tau \rangle_{(t,T)}, \tag{7}$$

where $\langle \tau \rangle_{(t,T)}$ is the mean travel time perturbation of the arrivals in the time window. Using (6) and (7) gives the maximum value of the cross-correlation

$$R^{(t,T)}_{\rm max} = 1 - \frac{1}{2}\overline{\omega}^2\sigma_\tau^2, \tag{8}$$

where σ_τ^2 is the variance of the travel time perturbation for waves arriving within the time window. This means that we can extract the mean and the variance of the travel time perturbations of the waves arriving in a time window.

For a constant change δv in seismic velocity and fixed locations of the scatterers, the mean travel time perturbation is given by $\langle \tau \rangle_{(t,T)} = -(\delta v/v)t$. When the time window is small ($T \ll t$), $\sigma_\tau = 0$. The velocity change follows from the time of the maximum of the time-shifted cross-correlation function:

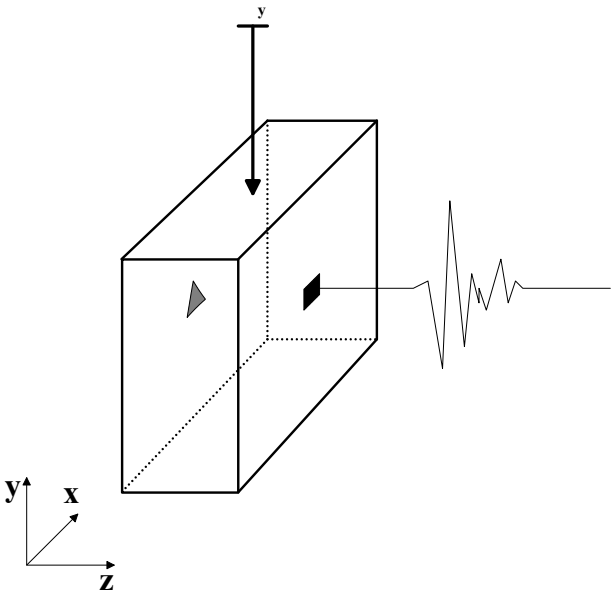

Figure 1. Experimental setup. The cuboid represents the Berea sandstone with orientation defined in the lower left corner of the figure. Sonic waves are transmitted in the z-direction and a uni-axial load is applied in the y-direction. A P-wave transceiver (triangle) and a P-wave receiver (rectangle) are used throughout the experiment. The cuboid has a size of 12,5 cm by 40 cm by 40 cm.

$$\frac{\delta v}{v} = \frac{-t_{max}}{t}. \tag{9}$$

In the following experiments we only consider the relative velocity change estimated from the coda of the ultrasonic measurements. However, other types of perturbations leave a different signature on the time shifted correlation coefficient (Snieder *et al.*, 2002) and could be used to monitor rock-properties not discussed here.

The laboratory experiments discussed in this paper are a combination of both, multiply scattering (from the cristals or grains in the rocks) and the repetitive sampling of the same area by reflections of the boundaries (bouncing ball and/or surface wave). However, the above formulation using the Feynman path summation includes both cases and we can use the same theory for all our measurements.

All the laboratory experiments discussed in this paper involve essentially the same measurement of ultrasonic waves, we measure the inpulse response of a rock sample with compressional ultrasonic transducers. The difference lays in the physics of the change introduced and the geometry of the rock sample.

Monitoring uni-axial stress in Berea sandstone

Time-varying stress fields are important in a number of areas of geophysics. Changes on plate boundaries are important in order to understand plate tectonics (Bokelmann & Silver, 2002). In earthquake prediction, the deformation field is important for understanding fault behavior and its relation to earthquake occurrence (Stein, 1999; Freed & Lin, 2001; Niu *et al.*, 2003). In hydrocarbon reservoirs, the stress field is changed by recovery operations. It is important to understand the temporal change for time-lapse reservoir monitoring (Teanby *et al.*, 2004). Or consider the "Room and Pillar" is a method of underground coal mining, in which approximately half of the coal is left in place to support the roof of the active mining area. Large pillars are left while rooms of coal are extracted. Monitoring the stress field in the pillars and roof is crucial in a safe mining procedure (Nikitin, 2003).

Wyllie et al. (1958) et al. measured ultrasonic P-wave velocity as a function of effective stress in water

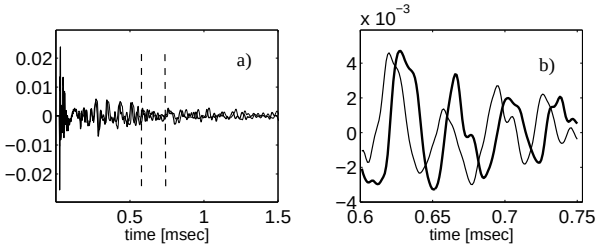

Figure 2. a) Two waveforms recorded at an applied uni-axial load level of 6 MPa (thick line) and 8 MPa (thin line) are shown in the same figure. b) The same two waveforms as Figure 3a, but only a small time window of the signal is shown; the time interval is marked by the two dashed lines in Figure 3a. The two coda waves are strongly correlated even. The sonic wave (in this time interval) has traveled through about 2.5 m of rock and bounced back and forth about 20 times.

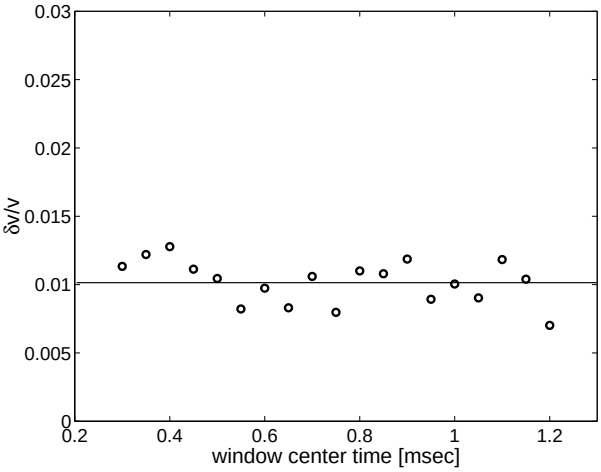

Figure 3. Velocity change estimates for 20 windows with different center times. The mean velocity change is 1.02 % and the standard deviation is 0.16 %

saturated Berea sandstone. They showed that at constant confining pressures v_p increases with decreasing pore pressure, and for constant effective stress the velocity remains constant. Similar relationships between effective stress and P-wave velocity have also been reported by others (Nur & Simmons, 1969; Hicks & Berry, 1956; King, 1966; Christensen & Wang, 1985). Experimental results indicate that confining and pore pressures have almost equal but opposite effects on v_p. Confining pressure influences the wave velocities because pressure deforms most of the compliant part of the pore space, such as micro-cracks and loose grain contacts. Closure of micro-cracks increases the stiffness of the rock and increases bulk and shear moduli. An increase in pore pressure mechanically oppose the closing of cracks and grain contacts, resulting in low effective moduli and velocities. Hence, when both confining pressure and pore pressures vary, only the difference between the two pressures has a significant influence on velocity (Hicks & Berry, 1956).

We first show how to use Coda Wave Interferometry for stress-field monitoring in a laboratory environment. In the following section we show the application of Coda Wave Interferometry in monitoring fluid saturation. In this experiment we use a fine-grained Berea sandstone to investigate the dependence of elastic waves to uniaxial stress. The sandstone block is equipped with an ultrasonic source (transducer) on one side and a receiver on the other (Figure 1). The transducer excites the rock with a pulse having a dominant frequency of 0.2 MHz, and a single receiver, with a sampling interval of 1 μs, records the propagated waves. To reduce the noise level, 512 traces are stacked for each stress level. A typical record is shown in Figure 2a.

To introduce a controlled change in the medium over time, the sandstone block is placed under a hydraulic press and a uni-axial load is applied (see Figure 1). The uni-axial load is monitored by a pressure sensor between rock and press. For each stress state (4, 6 and 8 MPa) the sonic measurement is repeated.

Figure 2a shows two waveforms superimposed, one at a load of 6 MPa and the other at 8 MPa. After about 0.5 ms, the waves have a noisy appearance. Taking a closer look (Figure 2b), however, we can see a strong correlation between the two, with one waveform being time-shifted with respect to the other. Thus, despite the noisy appearance of the coda waves, these waves carry information about the structure of the medium, information that can be used to infer the change of sonic velocity with applied pressure.

The change of P-waqve velocity caused by an increase in the load from 6 MPa to 8MPa, is inferred from the phase shift in the coda waves (Snieder *et al.*, 2002), using 20 non-overlapping 0.05ms time windows of the coda waves. Every window provides an independent estimate of the relative velocity change, that can be used for a consistency check of the method. Since we have multiple estimates of $\delta v/v$ we can calculate the mean and variance of the relative velocity change. The relative velocity change is of the order of 1.02% for a increase in load of 2 MPa with an error of 0.16% (Figure 3).

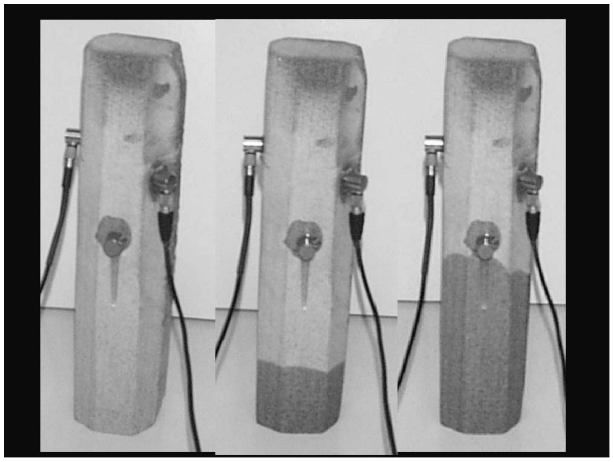

Figure 4. Three pictures of the berea sandstone sample, with ultrasonic source and receiver glued to the rock. The first picture from the left, shows the room dry sample. The second shows the water rising in the sandstone sample (dark line about a fourth up the sample) and the last picture shows the water almost half way up the rock. The third transducer glued to the rock is not used in this experiment.

Sarkar et al. (2003) showed comparable velocity changes in Berea Sandstone using traveltime-tomography based on first arrivals. In contrast to Coda Wave interferometry, tomography results can measure anisotropy, S- and P-wave velocity. However, the accuracy and sensitivity of Coda Wave Interferometry are an order of magnitude higher. On the other hand, since there is continual mode-conversion at boundaries and heterogeneities, the method cannot distinguish P- and S-wave velocity. In a Poisson medium however, a ratio between the two can be derived (Snieder, 2002).

Monitoring Water Saturation in Berea Sandstone

Seismic methods can monitor ground water (Bachrach & Nur, 1998), DNAPL (Dense Non-Aqueous Phase Liquid) contamination movement (Griffin & Watson, 2002), and hydrocarbon migration (Lumley, 1995) by detecting changes in seismic velocity. Compressional and shear wave velocities respond to changes in the bulk modulus, shear modulus and density caused by the presence of water. As stated above, an increase in pore pressure results in low effective moduli and velocities and opposes the effect of confining pressure. We demonstrate the application of Coda Wave interferometry for monitoring changes in water saturation in Berea sandstone.

We use an assymetrical piece of Berea sandstone

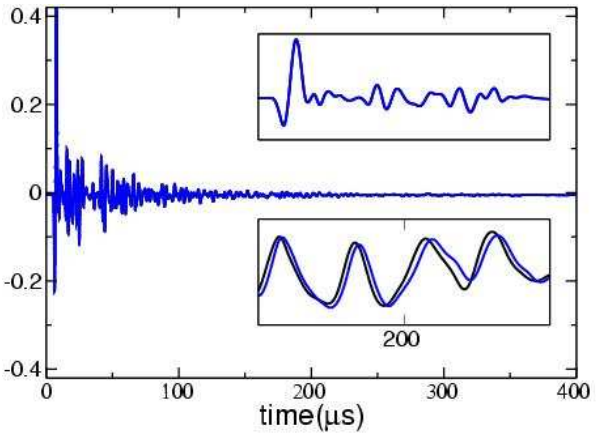

Figure 5. Wave-forms recorded in the berea sandstone sample for two different levels of water saturation (water infiltrated 2cm of the rock (thick line) and 3cm (thin line)). The insets show details of the wave-forms around the first arrival

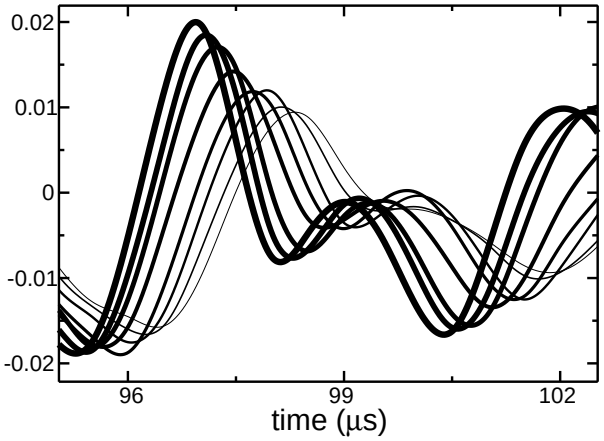

Figure 6. As the water rises in the rock sample the waves slow down accordingly. Eight waveforms are shown, each measured at a different hight of the water front. The fastest (thickest line) is measured on the dry sandstone and the slowest (thinest line) is measured at a water front hight of 7cm. It is important to note that the waveforms of the first arriving phases are identical for a water rise of 1cm.

with an approximate hight of 20 cm and an approximate diameter of 5 cm. The sample is equipped with a compressional source on one side and an identical receiver on the other (Figure 4). The room-dry sample is placed in a container holding 5mm of water. While the water is sucked into the pores of the sandstone by capillary pressure, the water-level in the container is kept constant at 5 mm. While the water-front is rising from 5mm to 10 cm, the ultrasonic impulse-response measurement is repeated for every 1cm increase in water-level. Again, for a 20 cm sample and a water-front rise of 1 cm there is no significant travel-time difference for

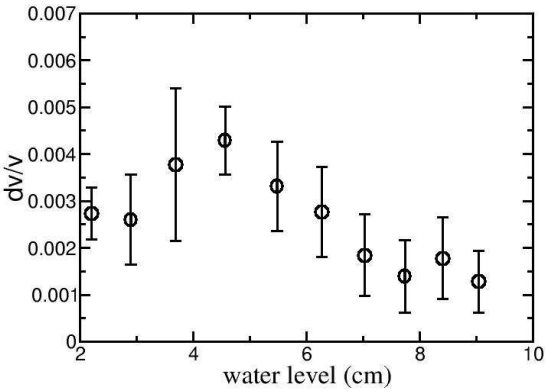

Figure 7. Absolute values of $\delta v/v$ in berea sandstone, for approximately 1cm water level intervals from room-dry to 9cm into the sample. Error bars are one standard deviation, calculated from multiple windows over the coda of the ultrasonic measurement

the first arriving waves (see top inset of Figure 5). In a late time window (bottom inset of Figure5), however, we see a distinct time shift of the wave-forms. Figure 6 shows the consistent slowing of the sonic waves with increasing water-level.

For each change of 1cm in water-level the relative change in velocity is estimated, with 12 different 0.1 ms time windows of the coda waves. The relative velocity change is of the order of 0.3% for a water-level rise of 1cm with an error of 0.05% (Figure 7). It is important to note that in many laboratory experiments, the change in the seismic velocity is measured for saturation changes of about 5% on small samples. With Coda Wave Interferometry we can monitor fluid saturation about 10 times more precisely.

Thus by using the coda waveforms, small changes in fluid saturation or migration, which have no effect on the first arriving phases of the data, can be readily seen in the coda. We believe that this technique can be used to monitor groundwater, DNAPL contamination sites and hydrocarbon reservoirs during enhanced recovery operations.

Monitoring Thermally Induced Velocity Changes in Aluminum

The dependence of ultrasonic velocity on temperature in metals and alloys is an important characteristic in

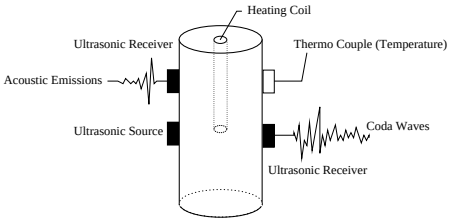

Figure 8. Experimental setup. The cylinder represents the Elberton granite or the aluminum sample. Sonic waves are transmitted through the sample. A longitudinal transducer, which excites primarily P-waves, and an identical receiver (right rectangle) are used throughout the experiment. A third identical P-wave transducer (top left rectangle) detects the acoustic emissions. The sample is heated with a heating coil placed in a centered borehole and the temperature is measured with a thermo-couple at the sample surface (white rectangle.)

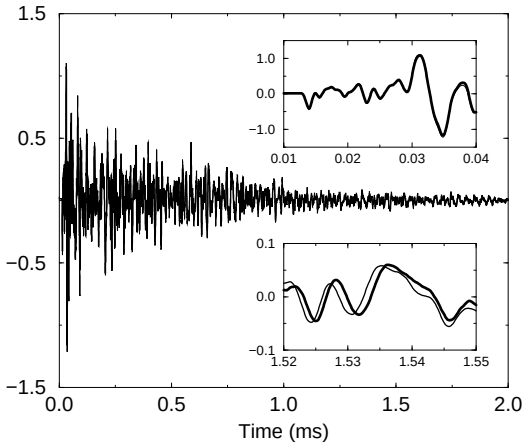

Figure 9. Wave-forms recorded in the granite sample for temperatures of 45^oC (thin) and 50^oC (thick) respectively. The insets show details of the wave-forms around the first arrival (top) and in the late coda (bottom.)

non-destructive testing (Kobori & Iwashimizu, 1990). Often, the effect of stress on this velocity/temperatur relationship is studied (Salama & Ling, 1980; Chern & Heyman, 1981). Further, multiply scattered or reverberating waves are known to be sensitive to such variations in temperature (Weaver & Lobkis, 2000). We use this sensitivity of coda waves to monitor temperature changes in aluminum.

In the ultrasonic experiment we use an aluminum cylinder with a hight of 11 cm and a diameter of 5.5 cm. The sample is equipped with an ultrasonic source on one side and a receiver on the other (Figure 8). The transducer sends a pulse through the sample, and the

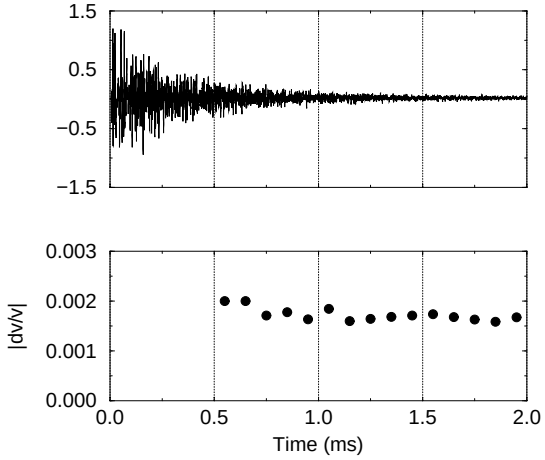

Figure 10. The top figure shows the ultra-sonic signal recorded on the aluminum sample. The bottom figure shows different estimates of $\delta v/v$ for multiple time-windows, therefore providing a consistency check. The early part of the signal is not used because it can't be considered a multiply scattered regime.

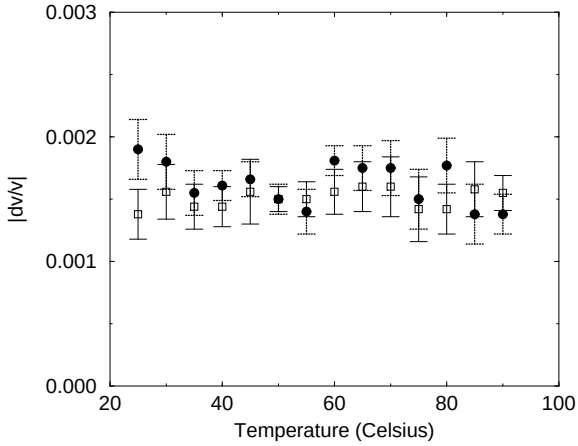

Figure 11. Absolute values of $\delta v/v$ in aluminum, for 5^oC temperature intervals from 25^oC to 90^oC. Circles correspond to the heating phase and rectangles (unfilled) to the cooling phase.

single receiver records the impulse response of the sample, with a sampling interval of 1μs (the dominant frequency is 100 kHz.) Ten traces are stacked to reduce the noise level. Two typical records for a cylindrical sample are shown in Figure 9.

To apply a controlled change in the medium over time, the aluminum sample is equipped with a heating element in a central borehole. The temperature is mon-

itored by two thermocouples glued to the side of the sample and in the borehole (Figure 8).

While increasing the temperature from 25^oC to 90^oC, the ultrasonic measurement is repeated for every 5^oC increase in temperature. Then the aluminum sample is cooled to room-temperature and the experiment is repeated again for every 5^oC in temperature decrease. In addition, acoustic emissions are counted for every temperature interval.

In some published laboratory experiments, the change in the seismic velocity is measured for a temperature change of about 100^oC (Kern *et al.*, 2001; Timur, 1977; Peselnick & Stewart, 1975; Hughes & Maurette, 1956). For a 11 cm small sample and a temperature difference of only 5^oC, there is no significant travel-time difference for the first arriving waves (see top inset of Figure 9). Therefore, first arriving waves do not provide any information about velocity changes. In a late time window (bottom inset of Figure 9), we see a distinct time shift of the wave-forms. This information can be used to infer the change of sonic velocity with temperature.

For each change of 5^oC in temperature the relative change in velocity is estimated with 20 different 0.1ms time windows of the coda waves 10. The relative velocity change is of the order of 0.15% for a temperature change of 5^oC with an error of 0.025% (Figure 11). It is important to note that the relative velocity change with temperature does not depend on whether the sample is in the heating or the cooling phase. Furthermore, there is no measurable velocity difference at room temperature before and after the sample has gone through the heating cycle.

This laboratory experiment is important to test the presence of temperature effects on the measurement equipment, like piezoelectric transducer, cables, transducer couplant or mounting devices. Since we measure a linear velocity change with temperature in aluminum (Weaver & Lobkis, 2000), we conclude that these effects can be neglected.

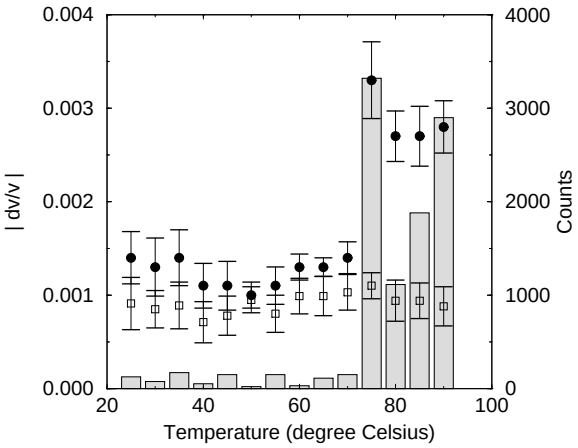

Figure 12. Absolute values of $\delta v/v$ in Elberton granite, for 5^oC temperature intervals from 25^oC to 90^oC. Circles correspond to the heating phase and rectangles to the cooling phase. The histograms show the count of acoustic emissions for a given temperature interval.

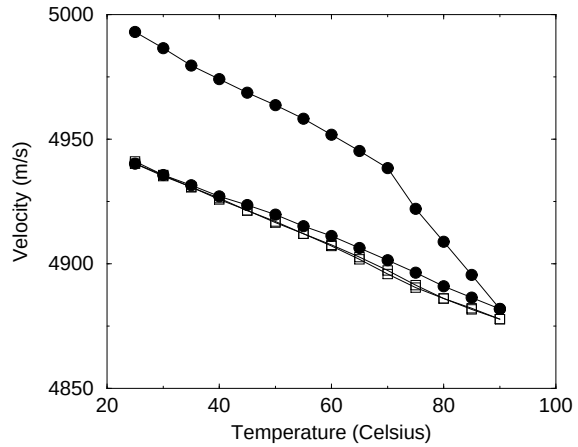

Figure 13. Absolute velocity versus temperature in Elberton granite, for two heating cycles. Filled circles represent the first heating cycle and rectangles the second. Note that on the second heating cycle the temperature dependent velocities during the heating and cooling phase are almost not distinguishable.

Monitoring Thermally Induced Velocity Change and Acoustic Emissions in Granite

With the same technique and same experimental setup described above, we measured the thermally induced velocity change in a granite sample. During the heating phase the velocity decrease is constant for each 5^oC increase in temperatures, below 70^oC, however for every 5^oC increase above that temperature, the velocity change is non-linear (Figure 12). A temperature of 70^oC corresponds to the critical fracture temperature for granite (Johnson *et al.*, 1978; Fredrich & Wong, 1986). Thermal cracking results from the internal stress concentration induced by thermal expansion anisotropy or thermal expansion mismatch between minerals or grains. Such micro-cracking is a similar effect as the thermal stresses induced by thermal gradients in homogeneous solids; for a high temperature gradient, cracking may occur even in a perfectly homogeneous solid (Boley & Weiner, 1960). Fredrich & Wong (1986) show that thermal cracking in rocks occurs principally along mineral or grain boundaries. The thermally induced cracks can influence significantly both the mechanical

and transport properties, as well as thermoelastic moduli (Simmons & Cooper, 1978).

In this experiment we use a third ultrasonic transducer in order to detect acoustic emissions in the granite due to thermal cracking. The histogramm in Figure 12 shows the count of acoustic emissions versus temperature. There is a small amount of acoustic emissions at low temperatures. However, there is a significant increase in acoustic emissions between 70^oC and 75^oC. The increase in velocity change and the jump in the number of acoustic emissions correlate well.

In (1953), Kaiser found that during repeated loading of metals, little or no acoustic emissions occurred until previously applied stress levels where exceeded. Since then, this effect has been known as the "Kaiser effect." Later, it was found that the Kaiser effect is a common phenomenon for various materials including rocks (Kurita & Fujii, 1979; Lavrov, 2002). Thus, the maximum stress applied in the previous cycles is 'memorized' in rocks.

During the cooling phase of the granite, there is a linear velocity change at 70^oC and there is only few acoustic emissions over the entire period. The seismic velocity does not increase back to its initial value at the end of the cycle. This difference in velocity is due to irreversible damage done to the rock by thermal cracking (Figure 13).

Todd (1973) studied the acoustic emissions of Westerly granite during cyclic heating. He noted that if a sample was re-heated to the same maximum temperature, few acoustic emissions occurred. Similarly we find in a second heating cycle up to the same maximum temperature (90^oC) for the same granite sample, only few acoustic emissions events occur and there is no nonlinear velocity decrease around 70^oC. Furthermore, the velocity increases back to the value before the second heating cycle when cooled down (Figure 13). Note, that there is a small difference in relative velocity change between the cooling phase of the first heating cycle and the second cycle. Thirumalai & Demou (1973) studied the residual strain in a granitic rock produced by cyclic heating, and showed that predominant damage took place during the initial exposure to heating and the damage reached a steady state after three successive heating cycles. If we increase the temperature above the previous maximum temperature (90^oC), the same non-linear effect will occur, the granite "remembers" the maximum temperature. This memory can only be erased by geologic time.

This indicates that two different mechanisms drive the temperature induced velocity change. The first mechanism is the change in bulk elastic constants with temperature, which is linear and reversible. This explains the constant velocity change with temperature during the second heating cycle during heating and cooling. The second mechanism is the damage done to the granite due to thermal cracking, which explains the nonlinear velocity change at the critical fracture temperature during the first heating cycle.

Ide (1937), found the same temperature dependence of velocity in Quincy granite. By means of first arrival travel time, he obtained 7 measurements over one heating cycle, with a peak temperature of 300^oC. With Coda Wave Interferometry we are able to measure twenty times more points over the same temperature interval.

Conclusions

Due to the sensitivity of coda wave interferometry, we are able to study the influence of changes in stress, temperature and fluid on small samples to a high level of precision. This would not be possible when ignoring the multiple sampling waves. The velocity estimation based on the coda waves requires only a single repeatable source and a single receiver. This means that one could monitor minute changes in-situ. In coda wave interferometry we have a technique to monitor a nuclear waste deposit in an inexpensive, automated and precise way. It might also be used, for example, as a diagnostic for non-destructive testing, volcano monitoring, land slides or monitoring of hydrocarbon reservoirs.

Acknowledgments

This work was partially supported by the NSF(EAR-0106668 and EAR-0337379).

REFERENCES

Aki, K. 1985. Theory of earthquake prediction with special reference to monitoring of the quality factor of lithosphere by the coda method. *Earthquake Res. Bull.*, **3**, 219–230.

Aki, K. 2000. Seismic monitoring and modeling of an active volcano for prediction. *J. Geophys. Res.*

Aki, K., & Chouet, B. 1975. Origin of Coda Waves: Source, Attenuation, and Scattering Effects. *J. Geophys. Res.*

Bachrach, R., & Nur, A. 1998. High-resolution shallow-seismic experiments in sand, Part I: Water table, fluid flow, and saturation. *Geophysics*, **63**, 1225–1233.

Bokelmann, G.H., & Silver, P.G. 2002. Shear stress at the base of shield lithosphere. *Geophys. Res. Lett.*, **29**(23), 2091.

Boley, B.A., & Weiner, J.H. 1960. *Theory of Thermal Stresses.* New York. Page 586 pp.

Chern, C.J., & Heyman, J.S. 1981. Determination of material stress from the temperature dependence of acoustic natural velocity. *Proceedings of the IEEE Ultrasonic Symposium*, 960.

Chouet, B. 1979. Temporal variation in the attenuation of earthquake coda near Stone Canyon, California. *Geophys. Res. Lett.*, **6**, 143–146.

Christensen, N.I., & Wang, H.F. 1985. The Influence of Pore Pressure and Confining Pressure on Dynamic Elastic Properties of Berea Sandstone. *Geophysics*, **50**, 207.

Fehler, M., Roberts, P., & Fairbanks, T. 1998. A temporal change in coda wave attenuation observed during an eruption of Mount St. Helens. *J. Geophys. Res.*, **93**, 4367–4373.

Fredrich, J.T., & Wong, T. 1986. Micromechanics of thermally induced cracking in three crustal rocks. *J. Geophys. Res.*, **91**, 12743–12764.

Freed, A.M., & Lin, J. 2001. Delayed triggering of the 1999 Hector Mine earthquake by viscoelastic stress transfer. *Nature*, **411**, 180–183.

Griffin, T.W., & Watson, K.W. 2002. A Comparison of Field Techniques for Confirming Dense Nonaqeuous Phase Liquids. *Ground Water Monitoring and Remediation*, **22**(2).

Hicks, W.G., & Berry, J.E. 1956. Application of Continuous Velocity logs to Determination of Fluid Saturation of Reservoir Rocks. *Geophysics*, **21**, 739.

Hughes, D.S., & Maurette, C. 1956. Variation of elastic wave velocities in granites with pressure and temperature. *Geophysics*, **21**, 277–284.

Ide, J.M. 1937. The velocity of sound in rocks and glasses as a function of temperature. *J. Geol.*, **45**, 689–716.

Johnson, B., Gangi, A.F., & Handin, J. 1978. Thermal cracking subjected to slow, uniform temperature changes. *paper presented at 19th U.S. Rock Mechanics Symposium, U.S. Nat. Comm. for Rock Mech., Univ. of Nevada, Reno.*

Kaiser, J. 1953. Erkenntnisse und Folgerungen aus der Messung von Gerüschen bei Zugbeanspruchung von metallischen Werkstoffen. *Archiv Eisenhüttenwesen*, **24**, 43–45.

Kern, H., Popp, T., Gorbatsevich, F., Zkarikov, A., Labanov, K.V., & Smirnov, Yu.P. 2001. Pressure and temperature dependence of V_P and V_S in rocks from the superdeep well and from surface analogues at Kola and the nature of velocity anisotropy. *Tectonophysics*, **338**, 113–134.

King, M.S. 1966. Wave Velocities in Rocks as a Functin of Changes in Overvurden Pressure and Pore Fluid Saturation. *Geophysics*, **31**, 50.

Kobori, O., & Iwashimizu, Y. 1990. *Effects of stress and temperature on ultrasonic velocity.* Elastic Waves and Ultrasonic Nondestructive Evaluation. Elsevier.

Kurita, K., & Fujii, N. 1979. Stress memory of crystalline rocks in acoustic emission. *Geophys. Res. Letters*, **6**, 9–12.

Lavrov, A. 2002. The Kaiser effect in rocks: principles and stress estimation technique. *International Journal of Rock Mechanics and Mining Sciences*, **40**, 151–171.

Lumley, D.E. 1995. *Seismic time-lapse monitoring of subsurface fluid flow.* Ph.D. thesis, Stanford Univ.

Nikitin, O. 2003. Mining block stability analysis for room-and-pillar mining with continuous miner in estonian oil shale mines. *Oil Shale*, **20**, 515–528.

Niu, F., Silver, P.G., Nadeau, R.M., & McEvilly, T.V. 2003. Migration of seismic scatterers associated with the 1993 Parkfield aseismic transient event. *Nature*, **426**, 544–548.

Nur, A., & Simmons, G. 1969. The Effect of Saturation on Velocity in Low Porosity Rocks. *Earth Planet. Sci. Lett*, **7**, 183.

Peselnick, L., & Stewart, R.M. 1975. A sample assembly for velocity measurements of rocks at elevated temperatures and pressures. *J. Geophys. Res.*, **80**, 3765–3768.

Revenaugh, J. 1995. The Contribution of Topographic Scattering to Teleseismic Coda in Southern California. *Geophys. Res. Lett.*, **22**, 543–546.

Salama, K., & Ling, C.K. 1980. The effect of stress on the temperature dependence of ultrasonic velocity. *J. Appld. Phys.*, **51**, 1505.

Sarkar, D., Bakulin, A., & Kranz, R. L. 2003. Anisotropic inversion of seismic data for stressed media: Theory and a physical modeling study on Berea Sandstone. *Geophysics*, **68**(2), 690–704.

Sato, H. 1988. Temporal change in scattering and attenuation associated with the earthquake occurence - a review of recent studies on coda waves. *Pure Appl. Geophy.*, **126**, 465–497.

Simmons, G., & Cooper, H.W. 1978. Thermal cycling cracks in three igneous rocks. *Int. J. Rock Mech.*, **15**, 145–148.

Snieder, R. 1999. Imaging and Averaging in Complex Media. *Pages 405–454 of:* Fouque, J.P. (ed), *Diffuse waves in complex media.* Dordrecht: Kluwer.

Snieder, R. 2002. Coda wave interferometry and the equilibration of energy in elastic media. *Phys. Rev. E*, **66**.

Snieder, R., Grêt, A., Douma, H., & Scales, J. 2002. Coda Wave Interferometry for Estimating Nonlinear Behavior in Seismic Velocity. *Science*, **295**, 2253–2255.

Stein, R.S. 1999. The role of stress transfer in earthquake occurrence. *Nature*, **402**, 605–609.

Teanby, N., Kendall, J.M., Jones, R.H., & Barkved, O. 2004. Stress-induced temporal variations in seismic anisotropy observed in microseismic data. *Geophys. Jour. Int.*, **156**, 459.

Thirumalai, K., & Demou, S.G. 1973. Thermal expansion behaviour of intact and thermal fractured mine rocks. *Am. Inst. Phys. Conf. Proc.*

Timur, A. 1977. Temperature dependence of compressional and shear wave velocities in rocks. *Geophysics*, **42**, 950–956.

Todd, T.P. 1973. Effects of cracks on elastic properties of low porosity rocks. *Thesis, Massachusetts Institute of Technology.*

Wang, Z. 1997. Feasibility of time-lapse seismic reservoir monitoring: The physical basis. *The Leading Edge*, **16**, 1327–1329.

Weaver, R.L., & Lobkis, O.I. 2000. Temperature Dependence of Diffuse Field Phase. *Ultrasonics*, **38**, 491–494.

Wyllie, M.R., Gregory, A.R., & Gardner, G.H.F. 1958. An Experimental Investigation of Fractors Affecting Elastic Wave Velocities in Porous Media. *Geophysics*, **23**, 459.